

1 Motion Management in Treatment Planning

1.1 Introduction

Effects of motion can have a significant impact on a radiation treatment (see Section ref!). Therefore a proper investigation is necessary for each specific treatment and patient. There are several motion mitigation techniques available that can operate on beam delivery, patient immobilization or treatment planning level.

One of the steps for motion mitigation is proper and frequent imaging. While most commercial treatment planning software provide rigid registration between different images, deformable image registration (DIR) is currently rarely used. Even though DIR better quantifies anatomical and biological variations [Sarrut, 2006] compared to rigid registration. DIR is essential as well in photon as in ion radiotherapy, with usage in adaptive radiotherapy [Yan et al., 1997, Yan,], 4D optimization [Trofimov et al., 2005], 4D dose calculation [Flampouri et al., 2006], contour propagation [Lu et al., 2006] and even in other categories besides radiotherapy as well [Cleary and Peters, 2010, Her, 2012, Nithiananthan et al., 2011, Naini et al., 2010]. Several different DIR algorithms are available, such as B-spline, Deamons, linear elastic finite element, optical flow, viscous fluid [Rueckert et al., 1999, Venugopal et al., 2005, Zhong et al., 2007, Thirion, 1998, Christensen et al., 1996], etc.

One of the reasons for the DIR is not used in commercial software is lack of proper DIR quality assurance (DIRQA). While several different DIRQA methods exist, none of them are definitive and most of them are time consuming. It is possible to evaluate DIR with deformable phantoms, where the type and size of deformation is known [Kashani et al., 2007, Kirby et al., 2011]. However such quality assurance is time consuming and cannot be used in everyday clinical workflow.

DIR validation can also be based on landmark positions, specifically their location before and after registration. In absence of externally planted markers, locating landmarks in patient anatomy can be time consuming and difficult to identify in low-contrast regions [Varadhan et al., 2013]. Another option is to compare delineated contours with the propagated ones. It is more efficient technique than landmark checks, however it is also time consuming and it does not address the region within the contour.

In this chapter tools to handle motion management, DIR and DIR validation will be presented. Tools were constructed for open-source software 3D Slicer, described in Section 1.2.1. In Section 1.2.2 details on how DIR was performed will be explained. Next, Section 1.2.3 will address

the DIR validation - an extensive tool was created with various features to tackle DIR validation. Section 1.2.4 will be about contour visualization. Last two sections in implementation part will be about a tool to display organ motion amplitude and generation of a mid-ventilation CT. Tools were tested on real patient data and results will be presented in the Section 1.3. Summary and discussion will be given last to sum up.

1.2 Implementation

1.2.1 3D Slicer

3D Slicer (Slicer) is a software platform for analysis and visualization of medical images [Slicer, 2016, Fedorov et al., 2012]. Slicer is a free, open-source software (BSD-style license) available on Windows, MacOSX and Linux operating systems. Slicer provides a vast variety of tools, such as:

- Handling a variety of image formats, including DICOM, NRRD and MHA
- Visualization of voxel images, polygonal meshes and volume renderings
- Registration tool (rigid and non-rigid) and display of vector fields
- Automatic image segmentation
- Analysis and visualization of diffusion tensor image data
- Device tracking for image-guided procedures

The foundation of Slicer is written in C++ and it's functions can be accessed also with Python to provide rapid, iterative development. Graphical user interface is built in Qt. Visualization is based on VTK, a graphical library commonly used in scientific research.

Slicer is a research tool and as such offers tools to implement new functionalities in the form of 3D Slicer extensions. They can either be as execution of external command-line programs or writing modules with new features or automate Slicer processes in form of scripted modules. In the next sections different Slicer modules will be presented, which were all developed in the scope of this thesis. The purpose of modules is to quantify and visualize patient motion as well as to provide quality assurance of the the obtained results.

1.2.2 Registration

The changes in patient anatomy can be seen on CT (4DCT) or MRI scan. To assest this changes a registration must be preformed. Registration can be made between different imag-

ing modalities, scans from different days or phases in 4DCT. Different algorithms and software is available for image registration. However, the result is always a transformation map [Richter, 2012].

$$x' = x + u_{ri}(x) \quad (1.1)$$

Here, x and x' are points in states r and i , respectively and u_{ri} is a vector field representation of the transformation map. u_{ri} can among others be used for assessing motion amplitudes, contour propagation and 4D dose reconstruction. It is important to note that for certain steps in 4D treatment planning require also inverse registration, from state i to r [Richter, 2012].

A commonly used software for registration in medical research is Plastimatch [Shackleford et al., 2010]. It is free and open-source software, available as a command-line executable program. Plastimatch B-spline registration is also available in Slicer as an external module, SlicerRT [Pinter et al., 2012]. The integration of Plastimatch in Slicer brings the advantage of a graphic user interface and hence a quick modification of parameters. However, the disadvantage comes when a large number of registrations is required, since a user presence is required. In a 4DCT registration there are $2(N - 1)$ registrations required - from reference phase to each of N states of 4DCT and vice versa, except for the reference phase itself. Typical 4DCT consist of 10 phases, therefore a automatic registration of a 4DCT is a necessity, since each registration takes from 15-30 minutes.

Rather than just automatically loading different phases and registering them in Slicer a patient hierarchy concept was introduced and is explained in Section 1.2.2.

Registration nomenclature

In order to be able to provide a clear description of methods and procedures used, an overview of the expressions used will be given here.

- **Reference image** - image that serves as a reference position.
- **Moving image** - image that is being registered to the reference image.
- **Warped image** - image resulting from registration. It should be as close to the image being registered to as possible.
- **True registration** - registration from moving to reference image. Similar, everything connected to true registration will use true(true vector field, true warped image, true absolute difference, true Jacobian, etc.).
- **Inverse registration** - registration from reference to moving image (opposite or inverse of true registration). As in true registration, term inverse can be used for everything con-

nected to it (inverse vector field, inverse warped image, inverse absolute difference, inverse Jacobian, etc.).

Patient hierarchy

Patient hierarchy follows a subject hierarchy principle in Slicer. It was designed for a clear overview of the registration process, DIRQA and all resulting files. Another reason is to track DIR and DIRQA in case if they are interrupted by Slicer crash. DIR and DIRQA files can be quite large and can cause Slicer to run out of memory. Patient hierarchy enables then to continue work from where it was interrupted.

There are several levels in patient hierarchy. Each level also has different attributes, where details such as file path or reference phase are written.

- Level 1: **Patient name** - separates different patients.
- Level 2: **Registration node** - separates between different registration, e.g. registration between 4DCT phases, between CT and 4DCT, MRI and CT...

The file directory of image, vector field and registration quality files is stored as an attribute. Additionally, there are number of phases to be registered and which phase is the reference one.

- Level 3: **Registration phase** - specific registration phase. Registration is done between all phases and the reference one. There have to be at least two phases
- Level 4: **Node** - can be either an image, a vector field, an inverse vector field or any of DIRQA nodes (see Section 1.2.3).

Exact file paths for specific node is stored as an attribute.

Patient hierarchy can be constructed in two ways. First option is to manually crate the whole patient hierarchy, from top to bottom level, with necessary attributes. Second option is using automatic script to look for files on hard drive and create corresponding levels in patient hierarchy. This is possible only, if some conventions are used regarding file names and locations.

1.2.3 Registration Quality Checks

In order to provide visual and quantitative assessment of the registration quality a **Deformable Image Registration Quality Assurance** module was created. It provides different image checks (false color, checkerboard, absolute difference, flicker, movie and landmark positions) and vector checks (Jacobian and inverse consistency error). Details on all different checks will be explained in this section. Reference image, warped image, vector and inverse vector (vector

from reference to moving phase) are used as inputs for DIRQA module. Additionally landmarks and region of interest (ROI) can be used as an input.

All checks that use some kind of mathematical operation on or between images (absolute difference, Jacobian and inverse consistency error) were built using tools from ITK library [Yoo et al., 2002].

False color

A good way to see difference between two images is to overlay them. However, since CT scans are usually displayed in grayscale color code, the differences can become indistinguishable. Especially if the images are quite similar, as reference and warped image usually are. With applying opposite color code to overlaying images two things are achieved. Firstly, regions where the registration was successful will be in grayscale. Furthermore the differences will be in color of image they belong to. In the module we used red and cyan color code for reference and warped image respectively. See Fig. 1.1 for details.

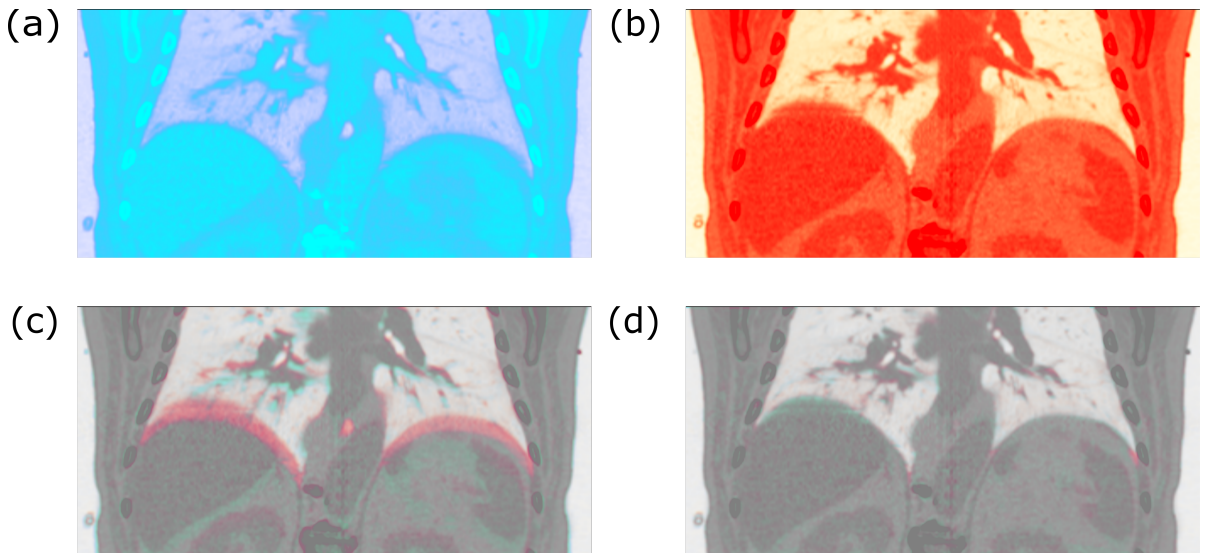


Figure 1.1: Example of false color overlay. Images (a) and (b) show red and cyan color code, respectively, for CT scan. (c) displays overlaid false colored images before and (d) after registration.

Checkerboard

As the name suggests, checkerboard creates an image of tiles. Each tile alternates between reference and warped image, as shown in Fig. 1.2. The differences between two images become apparent if there is no smooth transition from one tile to the next. The number of tiles can be manually selected. While the checkerboard offers clear indication of differences, it requires user to spot them - similar to false color.

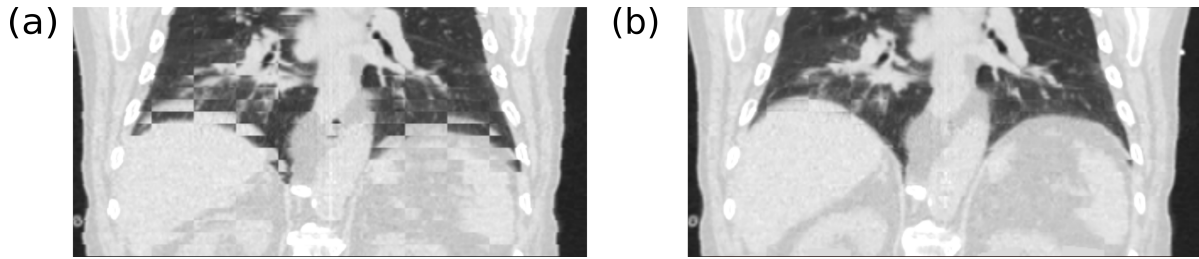


Figure 1.2: Example of checkerboard image. Image consist of tiles alternating between two images.

Tiles in image (a) alternate between scans before registration and in image (b) after registration.

Absolute difference

To stress the difference between reference and warped image an absolute difference between voxel values is calculated and displayed. New image is generated, with voxels populated as the absolute difference between reference and warped image voxel values, as shown in Fig. 1.3. Furthermore, average, standard deviation, minimum and maximum of absolute differneces are calulcated for quantitative assessment of registration quality (in ideal case all values would be 0).

The absolute difference feature is similar to false color, but it displays differences clearer and it also provides quantitative values. In contrast to false color which only relies on user examination.

To spare computational time or to focus on a specific region, absolute difference can also be calculated just on a specific ROI (if used as an input). Usually ROI around patient body is selected, rather than calculating on a whole patient CT.

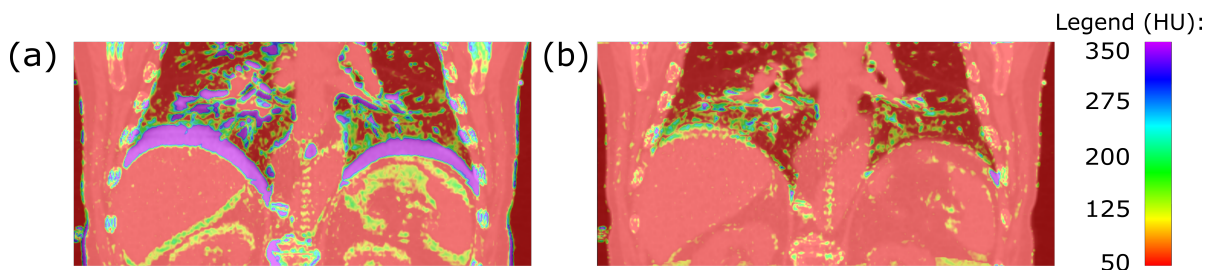


Figure 1.3: Absolute difference image before (a) and after registration (b). Image consist of tiles alternating between two images. Tiles in image (a) alternate between scans before registration and in image (b) after registration. The difference before registration is 350 HU and 100 HU after registration CHECK!

Movie

Medical images are usually quite large - typical CT image consist of $512 \times 512 \times 100$ pixels, which makes inspecting image checks (false color, checkerboard, absolute difference) a time-consuming task. Movie feature allows for smoother display of different image slices. User selects, which view he would like to inspect (axial, sagittal or coronal) and presses start. Selected views then start scrolling from one limit to the other. It allows user to focus on registration details, rather than scrolling through slices.

Movie and flicker (explained below) do not offer any specific registration check, but improve the process of registration quality assurance.

Flicker

While it is possible to display two images side by side in Slicer, it can sometimes be hard to see fine differences between the two images. Flicker alternates between reference and warped image on a single display. Flicker changes image each 0.5 s.

Landmark positions

Landmark positions are often used to determine registration spatial accuracy [Castillo et al., 2009]. Landmark can either be a specific feature in patient anatomy, or an external marker. The position of the landmark in the warped image would ideally be at the same position as in reference image. The module measures the Euclidean norm between the landmark position in reference and warped image.

User has to manually select landmarks in reference and moving image. For landmarks based on patient anatomy a physician is required. Landmark from moving image can then be automatically transformed with transformation vector field to obtain position in warped image or it can be manually selected in warped image.

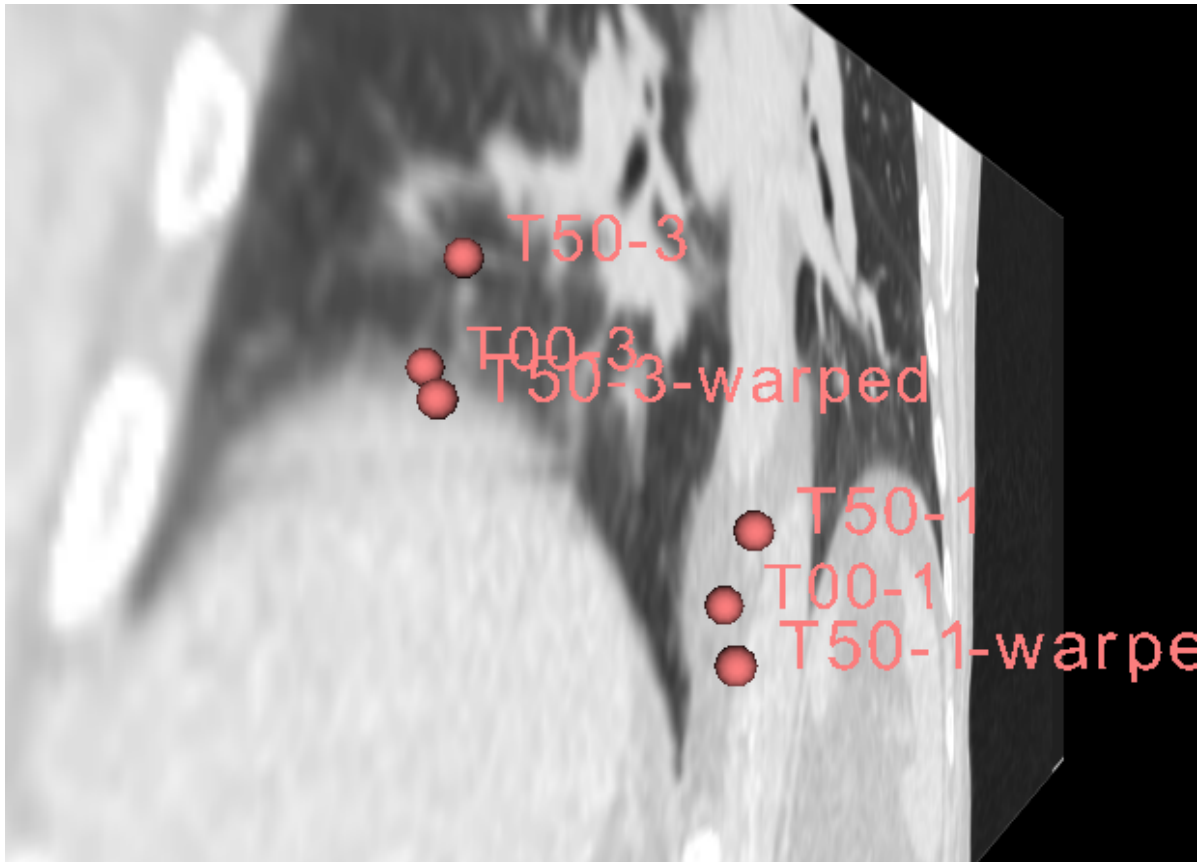


Figure 1.4: 3D display of landmarks in three phases - T00 and T50 (end-inhale and end-exhale, respectively) and T50 warped to T00 (T50-warped). Average distance of corresponding landmarks between T00 and T50 is 0.1 and between T00 and T50-warped is 0.1.

Jacobian

Jacobian determinant (Jacobian) of the vector field is used to validate physical behavior of registration [Leow et al., 2007]. Jacobian of vector field should be positive, since negative Jacobian values correspond to folding, which is physically unrealistic for patient anatomy (organs can not be folded) [Chen et al., 2008, Rey et al., 2002]. Expansions and contractions around a point are indicated by Jacobian values of greater and less than 1, respectively.

DIRQA module calculates and displays the Jacobian of the vector field. Average, standard deviation, minimum and maximum values of Jacobian are also displayed. Similar to absolute difference it also has ROI feature implemented.

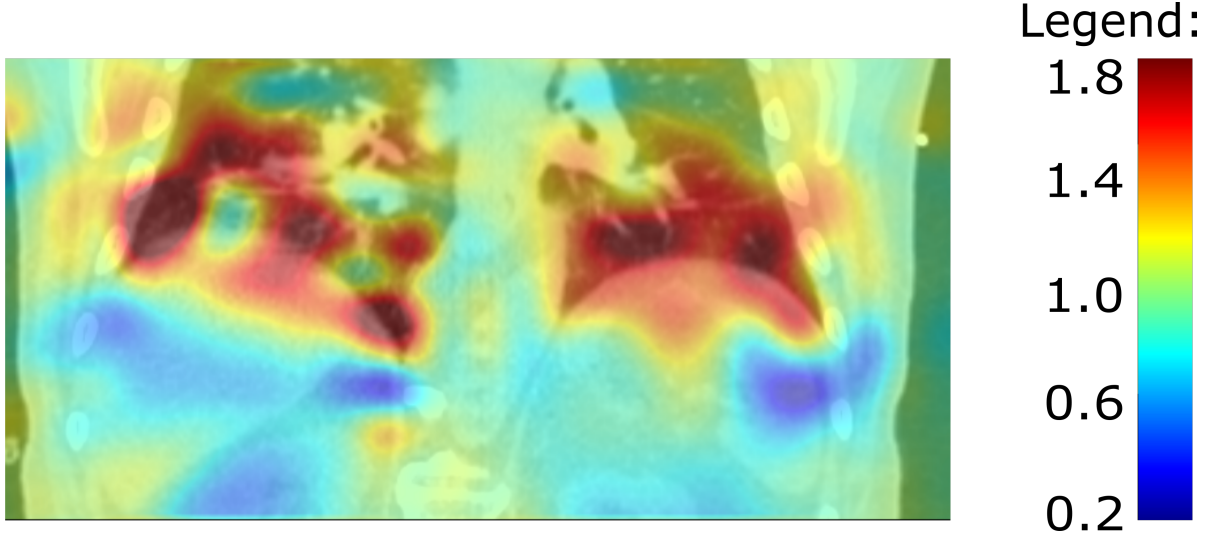


Figure 1.5: Image of Jacobian overlaid on CT scan. The average value of displayed Jacobian is 1.0 with 0.7 STD. CHECK!

Inverse Consistency Error

Inverse consistency error (ICE) is consistently used in literature as one of the main vector field checks **citati**. The principle is as followed. Suppose we have two vector fields - u_{AB} obtained from registration of image A to B and u_{BA} from registration of image B to A. The two registrations should be preformed separately. In ideal scenario, u_{AB} would be a direct inverse of u_{BA} . However, deformable image registration algorithms do not yield perfectly inverse consistent vector field.

To check for ICE, an algorithm was created that first transforms point x using u_{AB} . Newly obtained point x' is then transformed with inverse vector field, u_{BA} which yields x'' . The ICE is defined as Euclidean norm between x and x'' :

$$ICE = x - x'' = x - u_{BA}(x') = x - u_{BA}(u_{AB}(x)) \quad (1.2)$$

Points x' and x'' can have an arbitrary position in space, while vector fields u_{AB} and u_{BA} are positioned on a grid. To apply transformation $u_{BA}(x')$ a interpolation has to be made to put x' on a u_{BA} grid. A tri-linear interpolation is used in this module.

As in Jacobian, ICE image is calculated and displayed, along with values for average, standard deviation, minimum and maximum values. ROI feature is also implemented. An example is shown in Fig. 1.6

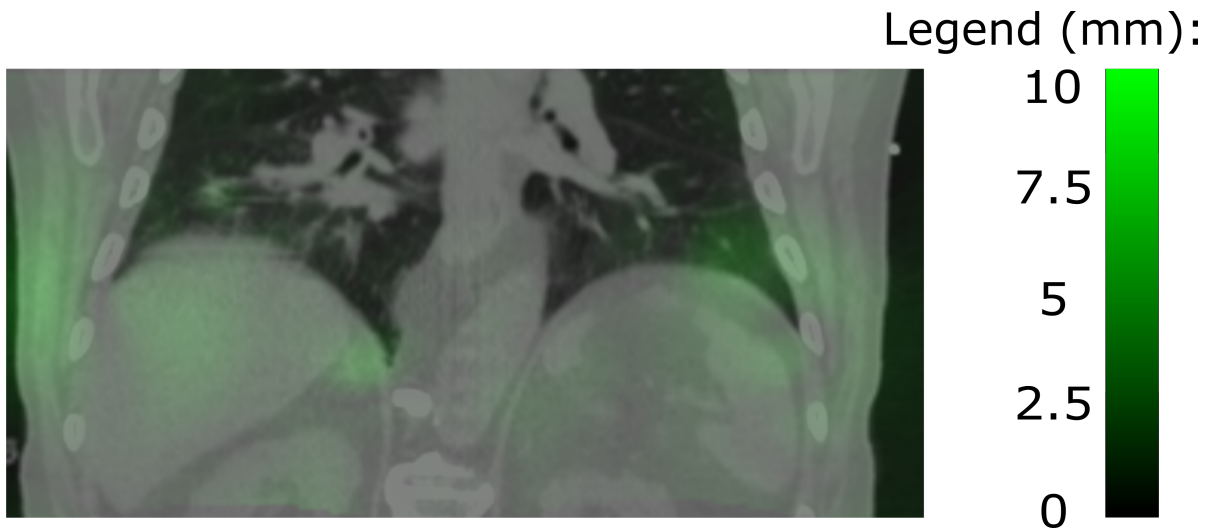


Figure 1.6: Image of inverse consistency error (ICE) overlayed on CT scan. The average value of displayed ICE is 1.0 with 0.7 STD. CHECK!

Output file

With all different features to validate DIR it can be time consuming to go through them all. A special option was created to automatically go through all different validation steps. Furthermore it can also run through different phases, if there are more phases (i.e. in 4DCT). All produced data from DIR validation is stored on disk and can be reexamined by user upon request. Furthermore, images are created and data is summed up and displayed in a separate file. Users can then preview file for first validation of DIR and then open necessary files, if required.

1.2.4 Contour visualization

TRiP4D (see Section [REF](#)) introduced volume datasets for contour representation [Richter, 2012]. It enabled necessary tasks for 4D calculations, such as the storing contour in different 4D states, contour propagation, etc. However, there was a lack of a proper visualization tool. In order to provide a contour visualization tool, a Slicer module was created.

Contours are saved as volumetric boolean masks. A single bit per ROI contour representation marks each voxel inside volume dataset [Richter, 2012]. To properly display contour, first a whole volume dataset was imported in Slicer. User selects which motion state he would like to inspect. The corresponding bit is then selected on the imported volume dataset. Lastly the contour is converted into 3D model shape.

1.2.5 Motion estimation and ITV creation

ITV is often created by an eye investigation of all 4DCT phases, where the extent of motion is estimated. Automatic creation of ITV is scarce in commercial system, since it requires DIR on all 4DCT phases. A Slicer module was created to assist with the motion estimation and automatic ITV creation using DIR.

Module is able to estimate and display motion of a user selected contour in three axis (left-right, anterior-posterior, superior-inferior) based on DIR vector fields. Module also performs DIR on 4DCT with patient hierarchy, if it has not been done yet.

Beside motion estimation, module can also propagate selected contour (usually CTV) and propagate it to all 4DCT and make a convolution of all propagated contours, resulting in automatically generated ITV.

Generation of mid-position phase

Most commercial software calculates treatment plan on a single 3D CT scan, using 4DCT only for motion estimation. To incorporate patient-specific motion information, a 3D CT scan was created from 4DCT in the time averaged position, also known as mid-position scan (midP scan) [Wolthaus et al., 2008]. With midP scan commercial software can still be used. Additionally, it also enabled smaller error margins for PTV generation and midP scan has less noise as individual 4DCT scans, because it uses more data.

Construction of a midP begins with registration of whole 4DCT. The resulting vector fields from reference position to 4DCT phases are then averaged to obtain mean vector field, see Fig. 1.7. Afterwards, for each vector field the mean vector field was subtracted, yielding a set of mean-corrected vector fields pointing from mean position to corresponding 4DCT phase. The mean-corrected vector fields were finally inverted and applied to each 4DCT phase, resulting in each phase being in the same, time-averaged position. In the end the set of transformed 4DCT phase was averaged to obtain midP scan.

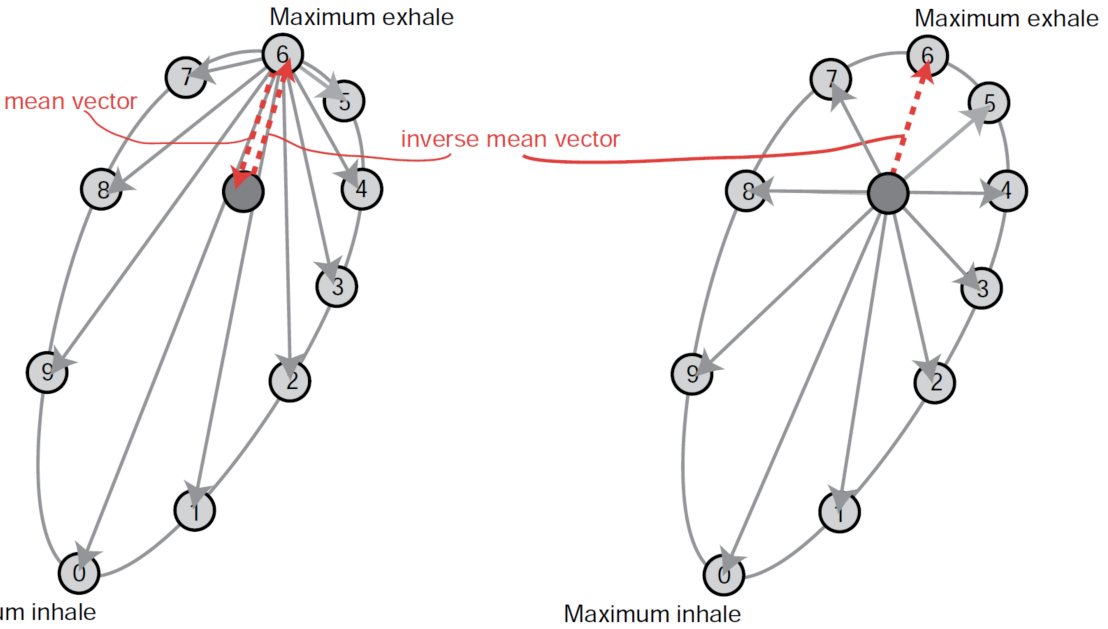


Figure 1.7: Computation of the midP scan. All vectors have the same starting point (reference phase, maximum exhale in this example), therefore they can be averaged, resulting in the mean vector. Next vectors from mean position to 4DCT phases have to be computed, which is achieved by subtracting original vectors and mean vector. Figure taken from [Wolthaus et al., 2008]

1.3 Verification

Several extensions for Slicer were created to tackle the issue of motion in treatment planning. With these extensions it is possible to perform DIR, DIR quality assurance, estimate organ motion and make midP scans. All extensions have to be checked on actual clinical data, to make future extension usage possible. Furthermore it is necessary to test if extensions could be used in a typical clinical workflow. Especially DIR validation, which is the reason for the lack of DIR in commercial treatment planning software.

DIR and DIR validation was done on lung 4DCT patient data. As part of a GSI pig-irradiation project (?) DIR and DIR validation was integrated in clinical workflow. Finally an example of midP scan on a liver cancer patient and its usage will be presented.

1.3.1 Registration of lung 4DCT patient data

Chapter **REF** and **REF** present studies on simulating active scanning carbon ion treatment (CiT) for lung cancer patient. The effects of interplay can drastically change the dose distribution for CiT and it is necessary to quantify effects of motion with DIR and transfer results into treatment planning software (TRIP4D in this case). An automatic procedure is required to perform DIR and

DIR validation on a large number of patients. This was achieved with Slicer modules described in Section 1.2.

Materials and Methods

A time-resolved CT (4DCT), consisting of 10 motion phases (0% - 90%) with resolution ? was acquired for 23 patients. Phase 0% corresponds to an end-inhale phase and was chosen as a reference phase.

DIR was preformed for each patient between each phase and reference phase and vice versa (true DIR and inverse DIR). For each patient 18 registrations were made, leading to 414 registrations in total.

DIRs were done with B-Spline Plastimatch module and patient hierarchy in Slicer (see Section 1.2.2 and 1.2.2). Two stages were used with details given in Table 1.1.

Table 1.1: Parameters used for Plastimatch registration. Details for each parameter can be found in [Plastimatch, 2016].

Parameter	Stage 1	Stage 2
Resolution	4,4,2	1,1,1
Grid size	50	15
Regularization lamda	0.005	0.005
Iterations	200	100

Absolute difference was computed for three image pairs: reference and moving image (default case), reference and moving warped image (DIR case), moving and reference warped image (inverse DIR case). Jacobian and ICE checks (see Section 1.5 and 1.2.3) were done on all 460 vector fields. To save memory usage all vector fields were rescaled by a factor of 2. ROI around patient body was manually created to get better results - area outside of patient is the same in all states and does not contribute to DIR. ROI was then used in absolute difference, jacobian and ICE.

For each patient it took around 1 h for all 20 DIR and **30 min** for complete DIRQA on all 20 DIR on Linux computer with 8 clusters and 16 GB RAM.

Results

DIR was successfully performed on all 23 patients. An example of DIR is shown on Fig. **DO IT**. Vector fields resulting from all DIR were analyzed and data is shown in Table 1.2. There was no statistical difference between true and inverse vector field. The biggest contribution to vector field magnitude was from superior-inferior direction (around 50%), then anterior-posterior direction (around 30%) and the smallest contribution was from left-right direction (around 20%).

Table 1.2: Data of vector magnitudes. Values are presented as average (range).

	True vector field	Inverse vector field
Mean	0.38 (0.01 - 1.28)	0.38 (0.01 - 1.3)
STD	0.95 (0.04 - 3.17)	0.98 (0.04 - 3.55)
Max	9.67 (0.61 - 28.56)	10.17 (0.56 - 37.11)

Data for absolute difference is shown in Figure and summarized in Table **DO IT**.

Jacobian and ICE results are shown on Fig. 1.8 and 1.2.3. Maximum values of true and inverse maximum and minimum jacobian and ICE were tested against maximum vector magnitudes and fitted with linear function. Resulting coefficients were 0.04 and -0.03 for maximum and minimum Jacobian, 0.04 and -0.02 for maximum and minimum inverse Jacobian and 0.4 for maximum ICE, respectively **Raj v tabelo?**. and were all statistically significant, with $p < 0.05$.

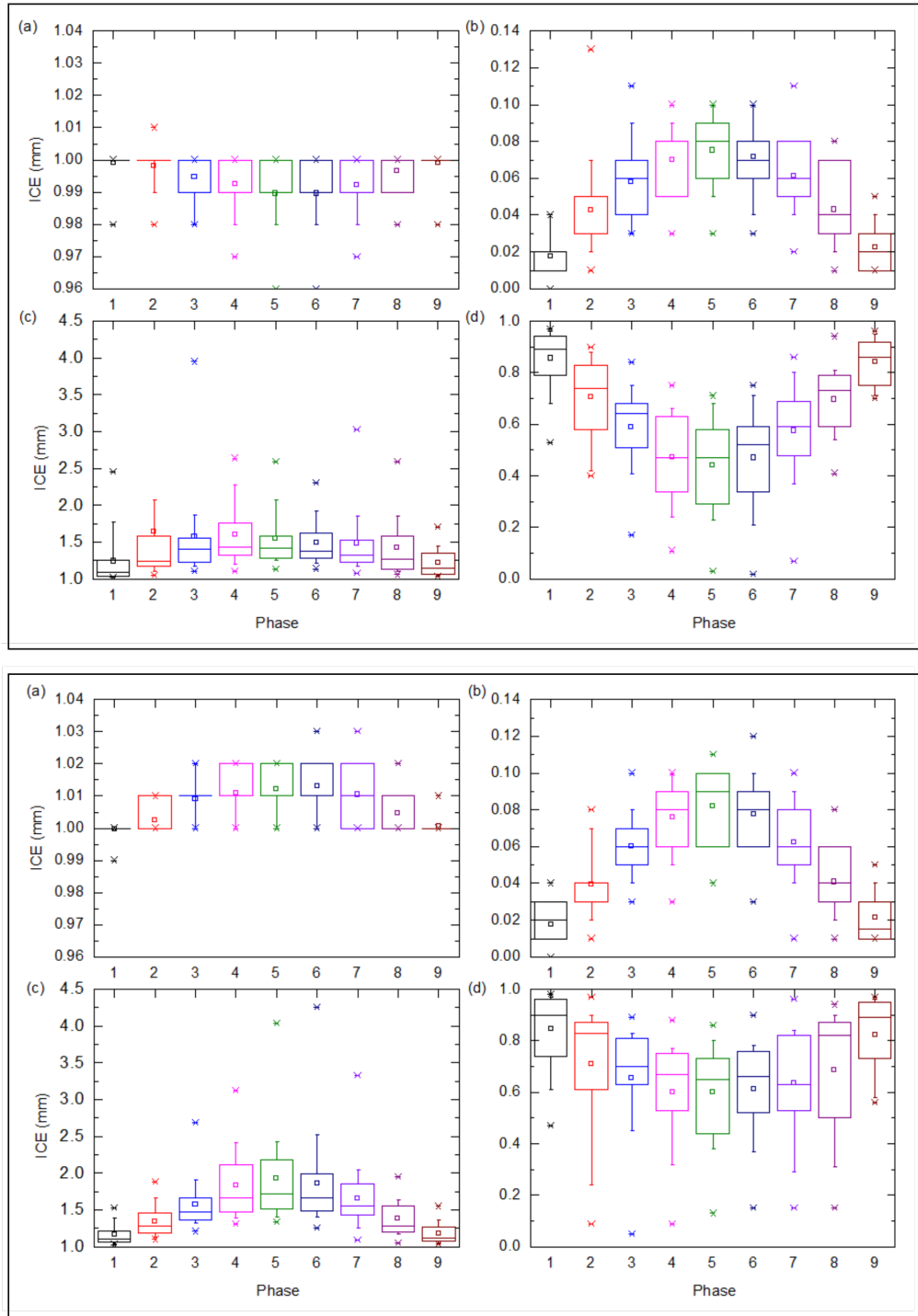


Figure 1.8: Data for Jacobian of vector fields (top) and inverse vector fields (bottom) for 9 4DCT phases (reference phase 0 is excluded) for 23 lung cancer patients. Mean, STD, maximum and minimum are represented as (a), (b), (c) and (d), respectively.

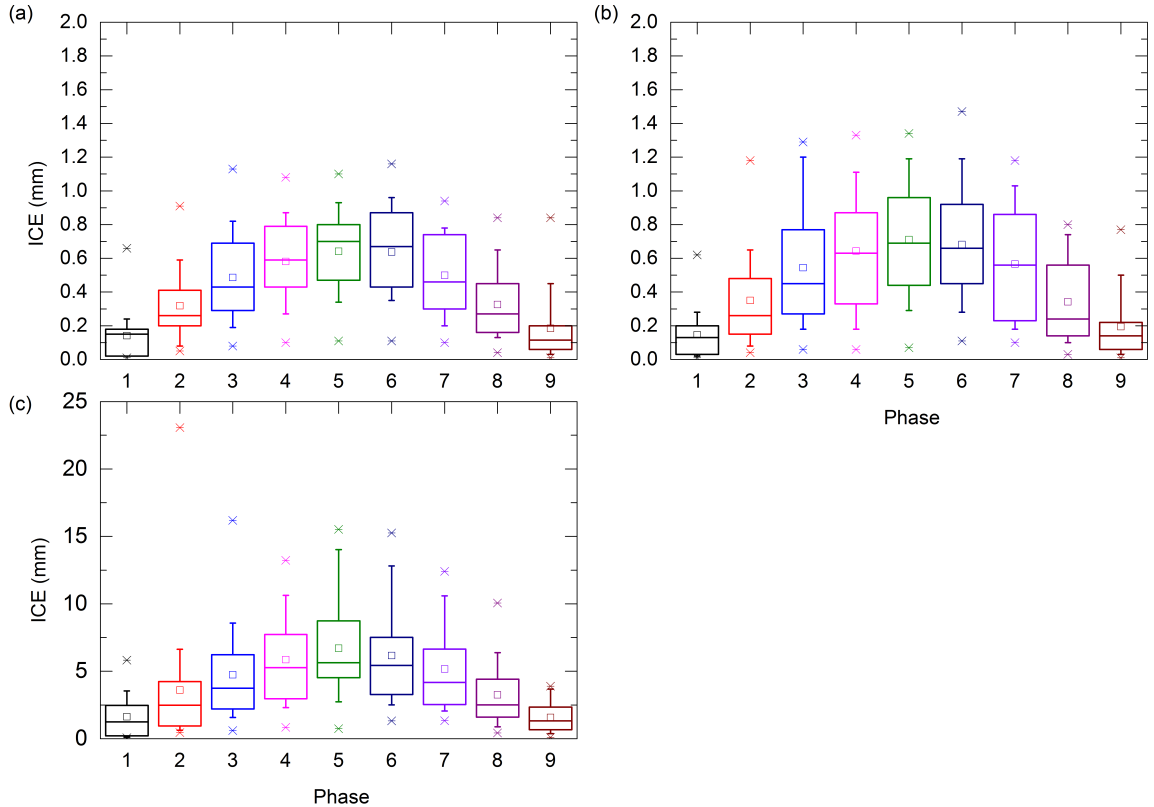


Figure 1.9: Data for ICE for 9 4DCT phases (reference phase 0 is excluded) for 23 lung cancer patients. Mean, STD, maximum are represented as (a), (b) and (c), respectively. ICE Minimum is 0 throughout all phases and patients.

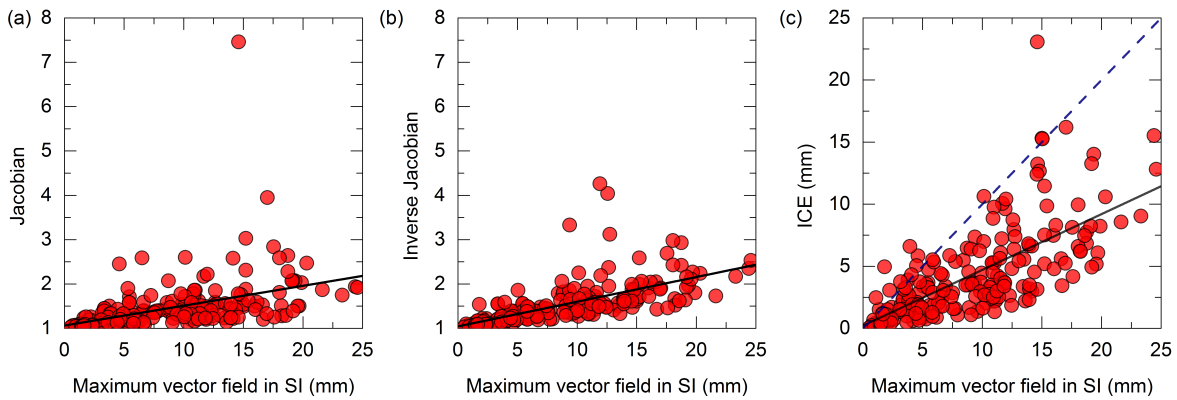


Figure 1.10: Maximum values of maximum jacobian (a), minimum jacobian (b) and ICE (c) versus maximum vector values (red squares) and maximum inverse vector values (green circles) in superior-inferior direction. Linear fit is displayed with red and green line for vector and inverse vector field, respectively. Dashed line in (c) shows $y(x) = x$ plot.

Discussion

Vector field magnitudes confirms previously published data that the biggest motion for lungs is in superior-inferior direction [Seppenwoolde et al., 2002, Britton et al., 2007, Liu et al., 2007]. The mean vector field magnitude is small (in submillimeter range), because the ROI included the whole patient body, not just the lungs where most of the motion occurs. There is little difference between values for vectors and inverse vectors, which was expected.

Values for Jacobian and inverse Jacobian were close to 1 with small STD, which indicates that most of the patient body does not change during the 4DCT scan. Mean values of maximum and minimum Jacobian were around 1.50 and 0.65 respectively, because there were expansions and contractions present. There were some extremely large values (7.46 the largest), that were result of an artifact present on a 4DCT scan, as shown on Fig **make that figure. Extremely low Jacobian?**. There is also a linear correlation between maximum and minimum (inverse) Jacobian and maximum vector field values as shown in Fig. 1.10. Large vector field values point to either expansion or contraction and resulting in large or small Jacobian values.

Following ICE definition in Eq. 1.2 there should be a correlation between vector field and ICE values. As such ICE mean and STD ICE are also in submillimeter range. The maximum ICE values can be large, with up to 2.3 cm, but still smaller as average maximum vector values. As shown in Fig. 1.10c a linear fit is a good approximation for maximum ICE dependence on maximum vector (inverse vector) field values. Furthermore, for first DIR check, ICE should always be lower as maximum vector field values. Cases above dashed lines in Fig 1.10c all have poor DIR, usually pointing to an artifact in the image.

As shown in Fig. 1.8 and 1.9 Jacobian, inverse Jacobian and ICE values follow motion curve for lungs (**PUT IT IN SECTION MID P**). The biggest difference for motion as well for Jacobian, inverse Jacobian and ICE is between extreme breathing positions, end-inhale (0%) and end-exhale (50%,60%).

1.3.2 Registration of pig heart 4DCT data

Atrial fibrillation is an unorganized atrial activity, causing a quivering motion of the heart. Heart is therefore not able to sustain a healthy pumping rhythm. Atrial fibrillation is not a deadly disease, however it worsens the patients quality of life and increases the risk of a stroke [Benjamin et al., 1998]. A common method for treating atrial fibrillation is catheter ablation [January et al., 2014], where the success rate is still limited and can even lead to major complications or even death of a patient [Cappato et al., 2005, R et al., 2010].

As an alternative treatment, a carbon-ion therapy was proposed [Bert et al., 2012] and later feasibility was shown experimentally [Lehmann et al., 2015b]. In 2014 ? a pilot experiment

was performed at GSI using large animal model (pigs) and scanned carbon-ion to verify treatment *in vivo*.

To estimate and compensate motion of the heart during irradiation DIR of 4DCT data was required. Furthermore, because of the actual irradiation of live pigs a DIRQA had to be made, to ensure validity of DIR. Description of procedure will be here, along with the results.

Materials and Methods

Pig irradiation experiment

A detailed description of pig irradiation experiment is given here [Lehmann et al., 2015a]. Here DIR and DIRQA used in the experiment will be presented. A cardiac gated contrast enhanced CT scans (4DCT-cardiac) were made on 15 pigs with a multidetector 64 row Siemens Somatom Definition Flash scanner (Siemens Healthcare, Forchheim, Germany). 1 mm voxel and 1 mm slice spacing were used. There was no breathing motion present, since a breath-hold technique was used. Cardiac motion was divided into 10 sequential phases (0-10%) and a field of view of 400 mm for skin-to-skin images was used.

After CT acquisition, DIR on 4DCT-cardiac phase was made using B-Spline Plastimatch module and patient hierarchy in Slicer (see Section 1.2.2 and 1.2.2). Details on parameters can be found in Table 1.3. Phase 0% was chosen as a reference phase. All other phases were registered to reference phase with inverse registration as well. An example of checklist for users to follow the right procedure is shown in Fig. 1.11a.

Based on lung patient DIR and because of the time pressure, DIRQA was made only on DIR from one phase, phase 50%. DIRQA consisted of absolute difference¹, Jacobian and ICE. DIRQA results were stored in a text file (example shown in Fig. 1.11b) and users checked if the values did not exceed expected ones: Absolute difference mean should be positive; Jacobian mean should be 1 with not too high extreme values; ICE mean should be smaller than 2 mm with not too high extreme values. ROI was manually created to encompass pig body and then used in all DIRQA checks.

After successful DIR and DIRQA vector fields were used in treatment planning and the resulting plans were used in pig irradiation experiment.

For each patient it took around 1 h for all 20 DIR on Linux computer with 8 clusters and 16 GB RAM.

¹ Relative difference between moving and warped image absolute difference was displayed in DIRQA file rather than just absolute values.

Table 1.3: Parameters used for Plastimatch registration. Details for each parameter can be found here [Plastimatch, 2016].

Parameter	Stage 1	Stage 2
Resolution	4,4,2	2,2,1
Grid size	50	15
Regularization lamda	0.005	0.005
Iterations	200	100

Post-experiment analysis

After pig irradiation experiment, a more detailed DIRQA was made, with all phases included in DIRQA. In addition to original checks explained in previous section, absolute difference checks were made on inverse warped image, Jacobian was made on inverse vector field and vector magnitudes were analyzed.

(a)

Checkliste Bestrahlungsplanung

DOSE: 406 TARGET: PV SCHWEIN: Uniform

Scripts path: AlXd/user/motion/Beamtime/GSI1407/Simulations/SCRIPTS

Heartbeats during CT: N:45 bpm Finalmotion: sin_3mm_1200ms0

Task	Script	Done?	Name	Date
Create Header		✓	AE	17.07.
Copy CT data to PatientData2		✓	AE	17.07.
Sort CTs (contrast/native)		✓	AE	"
Sort motion phased		✓	AE	"
Check # of files in each phase	CTX.sh	✓	AE	"
Check contrast and native slices	"	✓	AE	"
Create CTX	"	✓	AE	"
Create MHA	"	✓	AE	"
Check BB coordinates and write Header		✓	AE	"
Copy Contours		✓	AE	18.07.
Create VDX		✓	AE	"
Change 0 to 1 for Target (VDX)		✓	AE	"
Check voi names in VDX		✓	AE	"
FalseColorCheck contrast<->native (00)		✓	AE	18.07.
Contours native ok?				
Registration contrast -> 4DCT		✓	AE	17.07.
Registration ok?		✓	AE	17.07.

(b)

DIRQA for: Registration Node Contrast 4D

```

InvVector
x: 4.01
y: 3.59
z: 4.1
Vector
x: 4.53
y: 4.11
z: 4.49
AbsoluteDifference
Mean: 0.19
STD: 0.41
Max: 1446.0
Min: 0.0
Jacobian
Mean: 1.0
STD: 0.05
Max: 1.48
Min: 0.65
InverseConsistency
Mean: 0.11
STD: 0.17
Max: 1.97
Min: 0.0

```

Figure 1.11: (a) Part of the checklist for quality assurance during pig irradiation. DIR and DIRQA is highlighted in red and consisted of two steps. First DIR was made on 4DCT-cardiac and afterwards DIRQA was made on DIR on phase 50%. End result was presented as text shown in (b).

Results

An example of DIR is shown in Fig. **MAKEIT**. All DIR were successful and during experiment all DIRQA checks were positive. A vector field analysis is shown in Table 1.4. No statistical difference was observed between true and inverse vector field. Contributions to vector field magnitudes from three axis were equal.

Table 1.4: Data of vector magintudes. Values are presented as average (range).

	True vector field	Inverse vector field
Mean	0.07 (0.0 - 0.18)	0.07 (0.0 - 0.17)
STD	0.35 (0.05 - 0.78)	0.32 (0.04 - 0.71)
Max	7.13 (0.97 - 17.33)	6.57 (0.7 - 17.76)

Data for absolute difference is shown in Figure and summerized in Table **DO IT**.

Jacobian and ICE results are shown on Fig. ?? and ???. Maximum values of true and inverse maximum and minimum Jacobian and ICE were tested against maximum vector magnitudes. Linear fit was also obtained for results. and fitted with linear function. Resulting coeficents were 0.15 and -0.04 for maximum and minimum Jacobian, 0.08 and -0.05 for maximum and minimum inverse Jacobian and 0.9 and 0.95 for maximum ICE vs true and inverse vector field, respectively. All linear fits were statistically significant, with $p < 0.05$.

TJMax IJMax IJMin TJMin k = 1.63 1.8 1.71 n = -0.04 -0.07 -0.05 r = 0.90 0.80 0.90

Discussion

The mean vector field magnitude is almost zero, since the only motion is in the heart. The motion there is around 5 mm. There was no direction, that was dominant in terms of contribution to vector field magnitude.

Absolute difference?

On average the vector fields were almost zero, which results in mean Jacobian being 1. However, the extreme values of Jacobian deviated significantly from exected values - maximum Jacobian was **Fill in 17** and there were even 43141 cases of negative minimum Jacobian. This points to physically unrealistic scenarios (organ folding) which indicates invalidity of DIR. Furthermore the correlations on Fig. **YEH** and **DSE** are weak, supporting the

Values for Jacobian and inverse Jacobian were close to 1 with small STD, which indicates that most of the patient body does not change during the 4DCT scan. Mean values of maximum and minimum Jacobian were around 1.50 and 0.65 respectively, because there were expansions and contractions present. There were some extremely large values (7.46 the largest), that were result of an artifact present on a 4DCT scan, as shown on Fig **make that figure**. **Extremly low Jacobian?** There is also a linear correlation between maximum and minimum (inverse)

Jacobian and maximum vector field values as shown in Fig. 1.10. Large vector field values point to either expansion or contraction and resulting in large or small Jacobian values.

Following ICE definition in Eq. 1.2 there should be a correlation between vector field and ICE values. As such ICE mean and STD ICE are also in submillimeter range. The maximum ICE values can be large, with up to 2.3 cm, but still smaller as average maximum vector values. As shown in Fig. 1.10c a linear fit is a good approximation for maximum ICE dependence on maximum vector (inverse vector) field values. Furthermore, for first DIR check, ICE should always be lower as maximum vector field values. Cases above dashed lines in Fig 1.10c all have poor DIR, usually pointing to an artifact in the image.

As shown in Fig. 1.8 and 1.9 Jacobian, inverse Jacobian and ICE values follow motion curve for lungs (**PUT IT IN SECTION MID P**). The biggest difference for motion as well for Jacobian, inverse Jacobian and ICE is between extreme breathing positions, end-inhale (0%) and end-exhale (50%,60%).

1.4 Summary and Discussion

Bibliography

- [Her, 2012] (2012). Image-guided robotic surgery: update on research and potential applications in urologic surgery. *Curr Opin Urol*, 22(1):47–54.
- [Benjamin et al., 1998] Benjamin, E. J., Wolf, P. A., D'Agostino, R. B., Silbershatz, H., Kannel, W. B., and Levy, D. (1998). Impact of atrial fibrillation on the risk of death: the Framingham heart study. *Circulation*, 98(10):946–952.
- [Bert et al., 2012] Bert, C., Engenhart-Cabillic, R., and Durante, M. (2012). Particle therapy for noncancer diseases. *Medical Physics*, 39(4):1716–1727.
- [Britton et al., 2007] Britton, K. R., Starkschall, G., Tucker, S. L., Pan, T., Nelson, C., Chang, J. Y., Cox, J. D., Mohan, R., and Komaki, R. (2007). Assessment of gross tumor volume regression and motion changes during radiotherapy for non-small-cell lung cancer as measured by four-dimensional computed tomography. *Int. J. Radiat. Oncol. Biol. Phys.*, 68(4):1036–1046.
- [Cappato et al., 2005] Cappato, R., Calkins, H., Chen, S. A., Davies, W., Iesaka, Y., Kalman, J., Kim, Y. H., Klein, G., Packer, D., and Skanes, A. (2005). Worldwide survey on the methods, efficacy, and safety of catheter ablation for human atrial fibrillation. *Circulation*, 111(9):1100–1105.
- [Castillo et al., 2009] Castillo, R., Castillo, E., Guerra, R., Johnson, V. E., McPhail, T., Garg, A. K., and Guerrero, T. (2009). A framework for evaluation of deformable image registration spatial accuracy using large landmark point sets. *Physics in Medicine and Biology*, 54(7):1849.
- [Chen et al., 2008] Chen, M., Lu, W., Chen, Q., Ruchala, K. J., and Olivera, G. H. (2008). A simple fixed-point approach to invert a deformation field. *Med Phys*, 35(1):81–88.
- [Christensen et al., 1996] Christensen, G. E., Rabbitt, R. D., and Miller, M. I. (1996). Deformable templates using large deformation kinematics. *IEEE Transactions on Image Processing*, 5(10):1435–1447.
- [Cleary and Peters, 2010] Cleary, K. and Peters, T. M. (2010). Image-guided interventions: Technology review and clinical applications. *Annual Review of Biomedical Engineering*, 12(1):119–142. PMID: 20415592.
- [Fedorov et al., 2012] Fedorov, A., Beichel, R., Kalpathy-Cramer, J., Finet, J., Fillion-Robin, J.-C., Pujol, S., Bauer, C., Jennings, D., Fennessy, F. M., Sonka, M., Buatti, J., Aylward, S. R.,

- Miller, J. V., Pieper, S., and Kikinis, R. (2012). 3d slicer as an image computing platform for the quantitative imaging network. *Magn Reson Imaging*, 30(9):1323 – 1341.
- [Flampouri et al., 2006] Flampouri, S., Jiang, S., Sharp, G. C., Wolfgang, J., Patel, A. A., and Choi, N. C. (2006). Estimation of the delivered patient dose in lung imrt treatment based on deformable registration of 4d-ct data and monte carlo simulations. *Phys Med Biol*, 51(11):2763–2779.
- [January et al., 2014] January, C. T., Wann, L. S., Alpert, J. S., Calkins, H., Cigarroa, J. E., Cleveland, Jr., J. C., Conti, J. B., Ellinor, P. T., Ezekowitz, M. D., Field, M. E., Murray, K. T., Sacco, R. L., Stevenson, W. G., Tchou, P. J., Tracy, C. M., and Yancy, C. W. (2014). 2014 aha/acc/hrs guideline for the management of patients with atrial fibrillationa report of the american college of cardiology/american heart association task force on practice guidelines and the heart rhythm society. *Journal of the American College of Cardiology*, 64(21):e1–e76.
- [Kashani et al., 2007] Kashani, R., Hub, M., Kessler, M. L., and Balter, J. M. (2007). Technical note: A physical phantom for assessment of accuracy of deformable alignment algorithms. *Medical Physics*, 34(7):2785–2788.
- [Kirby et al., 2011] Kirby, N., Chuang, C., and Pouliot, J. (2011). A two-dimensional deformable phantom for quantitatively verifying deformation algorithms. *Medical Physics*, 38(8):4583–4586.
- [Lehmann et al., 2015a] Lehmann, H. I., C, G., A, C., P, L., M, P, D, R., M, T, A, E., R, K., P, S., Fiedler, F, S, H., C, F, N, E., R, R., AK, R., D, T, HA, K., SB, J., KD, P, J, D., T, H., S, A., C, B., M, D., and DL, P. (2015a). *Heart Rhythm*, volume Abstract. PO02-97, chapter Arrhythmia Ablation Using Scanned Carbon Ion Pencil Beams in a Porcine Model: First Outcomes from 12C Catheter-free Ablation.
- [Lehmann et al., 2015b] Lehmann, H. I., Richter, D., Prokesch, H., Graeff, C., Prall, M., Simoniello, P., Fournier, C., Bauer, J., Kaderka, R., Weymann, A., Szabó, G., Sonnenberg, K., Constantinescu, A. M., Johnson, S. B., Misiri, J., Takami, M., Miller, R. C., Herman, M. G., Asirvatham, S. J., Brons, S., Jäkel, O., Haberer, T., Debus, J., Durante, M., Bert, C., and Packer, D. L. (2015b). Atrioventricular node ablation in langendorff-perfused porcine hearts using carbon ion particle therapy: Methods and an in vivo feasibility investigation for catheter-free ablation of cardiac arrhythmias. *Circulation: Arrhythmia and Electrophysiology*, 8(2):429–438.
- [Leow et al., 2007] Leow, A. D., Yanovsky, I., Chiang, M. C., Lee, A. D., Klunder, A. D., Lu, A., Becker, J. T., Davis, S. W., Toga, A. W., and Thompson, P. M. (2007). Statistical properties of jacobian maps and the ralization of unbiased large-deformation nonlinear image registration. *IEEE Trans Med*, 26:822–832.

- [Liu et al., 2007] Liu, H. H., Balter, P., Tutt, T., Choi, B., Zhang, J., Wang, C., Chi, M., Luo, D., Pan, T., Hunjan, S., Starkschall, G., Rosen, I., Prado, K., Liao, Z., Chang, J., Komaki, R., Cox, J. D., Mohan, R., and Dong, L. (2007). Assessing respiration-induced tumor motion and internal target volume using four-dimensional computed tomography for radiotherapy of lung cancer. *Int. J. Radiat. Oncol. Biol. Phys.*, 68(2):531–540.
- [Lu et al., 2006] Lu, W., Olivera, G. H., Chen, Q., Chen, M. L., and Ruchala, K. J. (2006). Automatic re-contouring in 4d radiotherapy. *Phys Med Biol*, 51(5):1077–1099.
- [Naini et al., 2010] Naini, A. S., Patel, R. V., and Samani, A. (2010). Ct-enhanced ultrasound image of a totally deflated lung for image-guided minimally invasive tumor ablative procedures. *IEEE Transactions on Biomedical Engineering*, 57(10):2627–2630.
- [Nithiananthan et al., 2011] Nithiananthan, S., Schafer, S., Uneri, A., Mirota, D. J., Stayman, J. W., Zbijewski, W., Brock, K. K., Daly, M. J., Chan, H., Irish, J. C., and Siewerdsen, J. H. (2011). Demons deformable registration of ct and cone-beam ct using an iterative intensity matching approach. *Medical Physics*, 38(4):1785–1798.
- [Pinter et al., 2012] Pinter, C., Lasso, A., Wang, A., Jaffray, D., and Fichtinger, G. (2012). Slicerrt – radiation therapy research toolkit for 3d slicer. *Med. Phys.*, 39(10):6332–6338.
- [Plastimatch, 2016] Plastimatch (2016). <http://plastimatch.org>.
- [R et al., 2010] R, C., H, C., SA, C., W, D., Y, I., J, K., YH, K., G, K., A, N., Packer, D., Skanes, A., F, A., and E, B. (2010). *Circulation. Arrhythmia and electrophysiology.*, volume 3, chapter Updated Worldwide Survey on the Methods, Efficacy, and Safety of Catheter Ablation for Human Atrial Fibrillation, pages 32–38.
- [Rey et al., 2002] Rey, D., Subsol, G., Delingette, H., and Ayache, N. (2002). Automatic detection and segmentation of evolving processes in 3d medical images: application to multiple sclerosis. *Med Image Anal*, 6(2):163–179.
- [Richter, 2012] Richter, D. (2012). *Treatment planning for tumors with residual motion in scanned ion beam therapies.* Thesis/dissertation, TU Darmstadt.
- [Rueckert et al., 1999] Rueckert, D., Sonoda, L. I., Hayes, C., Hill, D. L. G., Leach, M. O., and Hawkes, D. J. (1999). Nonrigid registration using free-form deformations: application to breast mr images. *IEEE Transactions on Medical Imaging*, 18(8):712–721.
- [Sarrut, 2006] Sarrut, D. (2006). Deformable registration for image-guided radiation therapy. *Z Med Phys*, 16(4):285–297.

- [Seppenwoolde et al., 2002] Seppenwoolde, Y., Shirato, H., Kitamura, K., Shimizu, S., Lebesque, J. V., and Miyasaka, K. (2002). Precise and real-time measurement of 3D tumor motion in lung due to breathing and heartbeat, measured during radiotherapy. *Int. J. Radiat. Oncol. Biol. Phys.*, 53(4):822–834.
- [Shackleford et al., 2010] Shackleford, J. A., Kandasamy, N., and Sharp, G. C. (2010). On developing b-spline registration algorithms for multi-core processors. *Physics in Medicine and Biology*, 55(21):6329–6351.
- [Slicer, 2016] Slicer (2016). <https://www.slicer.org/>.
- [Thirion, 1998] Thirion, J. (1998). Image matching as a diffusion process: an analogy with maxwell's demon. *Med Image Anal*, 2(3):243 – 260.
- [Trofimov et al., 2005] Trofimov, A., Rietzel, E., Lu, H. M., Martin, B., Jiang, S., Chen, G. T., and Bortfeld, T. (2005). Temporo-spatial imrt optimization: concepts, implementation and initial results. *Phys Med Biol*, 50(12):2779–2798.
- [Varadhan et al., 2013] Varadhan, R., Karangelis, G., K., K., and Hui, S. (2013). A framework for deformable image registration validation in radiotherapy clinical applications. *J Appl Clin Med Phys*, 14(1).
- [Venugopal et al., 2005] Venugopal, N., McCurdy, B., Hnatov, A., and Dubey, A. (2005). A feasibility study to investigate the use of thin-plate splines to account for prostate deformation. *Physics in Medicine and Biology*, 50(12):2871.
- [Wolthaus et al., 2008] Wolthaus, J. W. H., Sonke, J.-J., van Herk, M., and Damen, E. M. F. (2008). Reconstruction of a time-averaged midposition ct scan for radiotherapy planning of lung cancer patients using deformable registrationa). *Medical Physics*, 35(9):3998–4011.
- [Yan,] Yan, D. Adaptive radiotherapy: Merging principle into clinical practice. *Seminars in Radiation Oncology*, 20(2):79 – 83.
- [Yan et al., 1997] Yan, D., Vicini, F., Wong, J., and Martinez, A. (1997). Adaptive radiation therapy. 42(1):123–132.
- [Yoo et al., 2002] Yoo, T. S., Ackerman, M. J., Lorensen, W. E., Schroeder, W., Chalana, V., Aylward, S., Metaxas, D., and Whitaker, R. (2002). Engineering and algorithm design for an image processing api: a technical report on itk—the insight toolkit. *Stud Health Technol Inform*, 85:586–592.
- [Zhong et al., 2007] Zhong, H., Peters, T., and Siebers, J. V. (2007). Fem-based evaluation of deformable image registration for radiation therapy. *Physics in Medicine and Biology*, 52(16):4721.

